# Possible techniques for particle size analysis in a $SiH_4$-$NH_3$ flame

Delft University of Technology
Faculty of Chemical technology and Materials Science
Department of Process technology
Section Particle technology and Risk management.

W. Oostra

supervisors:
Prof. B. Scarlett
Dr.Ir. J.C.M. Marijnissen
Ir. F.E. Kruis

December 1991.

**Content**

## 1.Introduction.

Recent interest in high temperature structural ceramics has led to the development of chemical vapour phase techniques for the formation of a variety of high quality ceramic powders. Silicon nitride, $Si_3N_4$, is one of the most promising materials of these structural ceramics, because of its high temperature strength, thermal shock resistance and corrosion resistance.

$Si_3N_4$ powders have been prepared by several techniques such as direct nitridation of silicon, decomposition of silicon diimide and vapour phase synthesis. Although, relatively small particles can be produced by using vapour phase synthesis initiated by convective heat [Lit.1], smaller and less agglomerated powders have been prepared using a sophisticated technique, Laser-Chemical Vapour phase Precipitation (L-CVP), developed by Haggerty and Danforth [Lit.2 ]. Characteristic of this laser-driven gas phase process is a well defined reaction zone which should facilitate a considerable degree of control over composition, size and size distribution of the produced powders.

This report gives the results of a literature study performed to investigate the possible techniques for particle size analyses in this reaction zone. The aim of this research is to get a better understanding of the processes taking place in this zone. This particle size analysis is to be performed in a flame of $SiH_4$ and $NH_3$ which is used in the production of $Si_3N_4$. The ideal technique measures a particle size distribution in-situ, in the submicron range, is cheap, easy to handle, fast and does not influence our process. The second chapter handles on techniques which use a form of light to determine the psd and are non-intrusive. The third chapter deals with techniques which require sampling, and some possible ways of sampling are reported. Chapter 4 deals with techniques which do not belong to the first two groups. Since thermophoresis can become an important phenomenon in our setup the last chapter deals with this phenomenon.

## 2. In-situ measurements using light.

### 2.1 Laser scattering extinction measurements

In literature many applications of light scattering techniques for particle size analysis are reported [Lit. 3, 4]. Scattering measurements have some obvious advantages : it is a non intrusive technique, and it is fast.The measured optical properties can be used to determine the particle properties using results from electromagnetic theory for spherical particles. The value of $Q_{vv}$, which is the scattering cross-section applicable for the vertically polarized scattered light, is calculated by summing the scattered cross-section for each particle of diameter $d_p$, multiplied by its relative frequency of occurrence. In the Rayleigh limit, when $d_p$ is much less than the wavelength of the scattered light $\lambda_0$, the value of $Q_{vv}$ for any $\Theta$ which is the scattering angle from the incident beam, is

$$Q_{vv} = \frac{F(m)}{4} \cdot \left(\frac{\pi}{\lambda_0}\right)^4 \cdot N \cdot \int_0^\infty P(d_p)\, d_p^6\, d(d_p) \qquad (1)$$

where

$$F(m) = \left|\frac{m^2-1}{m^2+2}\right|^2 \qquad (2)$$

and $P(d_p)$ is the particle size probability function, m the complex refractive index of the particle material, and N the total number of particles per unit volume. As can be seen these formula's are a strong function of the refractive index which itself is a strong function of the chemical composition of the particles. Furthermore problems arise when the measured particles are non-spherical or whenever the number-concentration is high.

### 2.2 Size and concentration measurements by means of a double extinction technique.

Gougeon [Lit 5] reports on a technique which measures particle size and concentration simultaneously in dense two-phase flows where multiple scattering phenomena are significant. The medium he studied was a cloud of coal particles with a number density of $10^8$-$10^{10}$ $m^{-3}$. He mainly concentrates on particles in the size range from 10 to 100 $\mu$m. He makes use of a He-Ne-laser ($\lambda = 0.6\ \mu$) and a self made HCN far-infrared laser ($\lambda = 337\mu$). He considers a slab (width: W) formed of Mie scatter centres surrounded by a non-absorbing medium having the same refractive index as the medium around the slab. The slab is illuminated by a pure collimated beam which interacts with the slab. He defines the collimated-collimated transmittance

In-situ measurements using light

$\tau_{cc}$ as the collimated transmitted energy over the collimated incident energy. When $Q_{ext}$ is the extinction efficiency factor depending on $d_p$, $\lambda$, and m, then the transmittance $\tau_{cc}$ is given by the Lambert-Beer law:

$$\tau_{cc} = \exp\left[-N \cdot \frac{\pi d_p^2}{4} \cdot Q_{ext}(d_p,\lambda,m) \cdot W\right] \qquad (3)$$

$Q_{ext}$ is a strong function of the particle diameter at $\lambda = 337\ \mu$, and equal to 2, its asymptotic value, at $0.6\ \mu$. When the two transmittances are measured simultaneously and the index of refraction is known the particle diameter can be calculated. Using this calculated diameter the number density is calculated from:

$$N = -\frac{4 \cdot \mathrm{Ln}\tau_{cc}}{\pi \cdot d_p^2 \cdot Q_{ext} \cdot W}$$

2.3 Diffusion broadening spectroscopy.

Driscoll [Lit.6] used diffusion broadening spectroscopy (DBS) to measure particle sizes in the range from 40 to 250 nm at 2200 K in a flowing gas. DBS is also referred to as Photon Correlation Spectroscopy (PCS) or Time Correlation Spectroscopy and Quasi Elastic Light Scattering (QELS). In this technique the particle size is determined by measuring the spectral broadening of scattered laser light. Broadening of the observed optical spectrum is a result of two factors : the vigorous diffusion of particles due to their Brownian motion and the Doppler effect. Therefore the diffusion coefficient can be determined directly from a measurement of the half width of the optical spectrum. Particle size is then inferred using a modified Stokes-Einstein relation that relates the diffusion coefficient and the particle diameter. Driscoll did correct for aerosol polydispersity and free molecular flow effects. The equation from which the diameter d is determined is :

$$d_p = \frac{16}{3} \cdot \frac{kT}{\lambda_o^2 \cdot \eta} \cdot \sin^2\left(\frac{\Theta}{2}\right) \cdot \frac{C}{HW} \qquad (5)$$

Where $\eta$ is the viscosity, $\lambda_0$ is the wavelength of the incident beam, C the Cunningham slip correction factor given by Fuchs, and HW the half width of the spectrum measured at half height in Hertz.
Driscoll does not mention the index of refraction of the medium in his work, though this is a very important parameter. The index of refraction should be in the nominator of equation (5) with a power of 2.
When the index of refraction of the particles is known it is also possible, when two angles are measured, to determine particle size distribution parameters as geometric mean and standard deviation of a log-normal distribution.

In-situ measurements using light

He calculated the halfwidth of the spectrum for different size distributions at two angles and plotted the ratio of these values against the geometric standard deviation for different values of the mean diameter. The geometric mean of a distribution is now calculated from (5) and the standard deviation is then determined from the figure. Ohsawa [Lit 7] used the FFT-variant of DBS to measure particle diffusion coefficients in the order of $10^{-9}$ $m^2/s$, the corresponding diameter depends very much on the used relation between diffusion coefficient and diameter.
Ohsawa uses

$$r = \frac{8}{3} \cdot \frac{kTm^2}{\lambda_0^2 \eta} \cdot \sin^2\left(\frac{\theta}{2}\right) \cdot \frac{C}{HW} \qquad (6)$$

to determine particle radius r from the measured half-width of the spectrum. This formula is essentially the same as Driscoll uses, apart from the index of refraction of the medium m. Ohsawa used a 100 mW Argon ion laser ($\lambda =$ 514.4 nm) and his detection volume consisted of a cylinder with a length of 25$\mu$m and a diameter of 25$\mu$m.

2.4 Two dimensional laser light scattering.

Cavaliere [Lit.8] reports on a two dimensional laser light scattering technique which he used in the study of atomization and dispersion processes in unsteady diesel sprays. He was able to get information on the inner part of the spray. In this technique the beam of a 532 nm pulsed laser is shaped in to a thin sheet 200 $\mu$m thick through a set of cylindrical lenses. The sheet is spatially filtered in order to transmit only the uniform part of the laser. The scattered light is collected perpendicularly to the laser sheet. After several filtering steps he makes use of a bundle of fibre-optics and a lens set to focus an image on a ccd-monoshot camera. The frames are then digitized and the dark field signal is eliminated through subtraction of a background. Though this technique is yet not capable of being linked to physical quantities (particle size) he was able to distinguish 5 sequential fragmentation processes, in the atomization, at different distances from the nozzle.
2.5 Multiple-wavelength pyrometer measurement of particle size.

All techniques above used an external light source to determine particle size, in flames another option is to use the emitted radiation from the flame itself to determine the psd. Mackowski [Lit.36] used a pyrometer which measured flame emission and extinction at 1.6, 2.3, 3.8, and 4.4 $\mu$m to determine particle and gas temperature and the ratio of the third to second moment of the size distribution function.
An expression for the emitted flame intensity at the gas-transparent wave length is:

$$I_\lambda = \left(1 - e^{-\kappa_\lambda W}\right) I_{b\lambda} \qquad (7)$$

where $\kappa_\lambda^p$ is the particle absorption coefficient, $I_b$ is the black-body intensity, $I_\lambda$ is the intensity at wavelength $\lambda$ and W is the path length. At 4.4 $\mu$ which is within a gas absorption band the emitted intensity is given by:

$$I_{4.4} = \frac{\kappa_{4.4}^p I_b^p + \kappa_{4.4}^g I_b^g}{\kappa_{4.4}^p + \kappa_{4.4}^g}\left(1 - e^{(\kappa_{4.4}^p + \kappa_{4.4}^g)W}\right) \qquad (8)$$

where superscripts p and G denote particle and gas, respectively. For the relation between $\beta_\lambda{}^p$ and $\kappa_\lambda{}^p$ and the concentration, refractive indices and the third to second moment of the size distribution of dispersion he used an empirical correlation. For the concentration he assumed ideal gas behaviour and an expression for the gas absorption coefficient is obtained from:

$$\left(\frac{\beta_{4.4}}{\beta_{3.8}}\right)_{meas} = \frac{(\beta_{4.4}^p + \kappa^g)}{\beta_{3.8}^p} \qquad (9)$$

The left-hand side of Eqn. (9) represents the ratio of the measured extinction coefficients , whereas the particle absorption and extinction coefficients appearing on the right hand side are calculated with the empirical correlation. Measuring at 4 wavelengths yields 8 equations with 8 unknowns, this he solved using a non-linear least-square-error code. The coal particles he feeded were in the size-range 10-26 $\mu$ but he measured lower values due to soot formation, soot is normally in our size range.

## 2.6 Summary.

Most of the techniques treated in this chapter are in principle suited for our application. But for most techniques, the time required for implementing and understanding the technique can become quite long. Most techniques require a specialist to guarantee reliable results and therefore non of them is a realistic option at this moment.

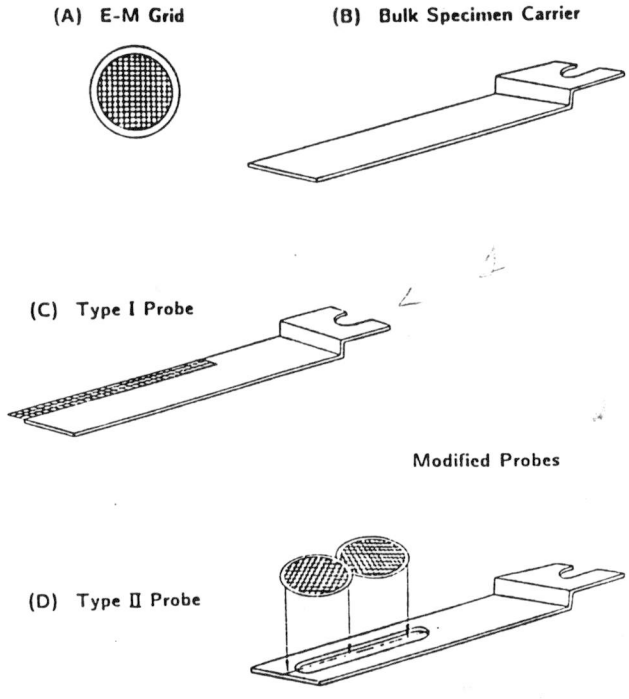


Fig. 1,2 Probes used by Dobbins

## 3. Sampling techniques.

### 3.1 thermophoretic sampling

Thermophoretic deposition is driven by the presence of a temperature gradient in the vicinity of a cold wall inside the flowfield of a particle laden gas. This gradient is readily established by introducing briefly into the hot flame gases a probe surface which is initially at room temperature. When thermophoresis is the main deposition mechanism (a) nearly all particle sizes will be captured with approximately equal efficiency, (b) little coagulation can be expected in the thermal boundary layer since, in this particle range, there is no differential (size dependent) thermophoretic drift. The exposure time $\tau_e$ should be long enough to capture a significant sample but short enough to present a cold surface to the flame born particles. This cold surface serves a second important purpose which is that it freezes heterogeneous reactions of the particles that are already captured. In literature many authors report of using thermophoretic sampling for deposition of soot. In most cases it is simply a wire which is kept in the flame for a certain time. In 2 cases a more refined system is used these two will be dealt with in this chapter.

#### 3.1.1 A pneumatic cylinder

Dobbins [Lit.9] designed an apparatus which enables him to expose probes for thermophoretic sampling to flames for times as short as 30 ms. His probe system consists of a double acting pneumatic cylinder driven by an air pressure of 4.5 atm, the probe trajectory is recorded by a linear transducer. For analysis of his particles he used SEM and TEM techniques. To combine these two techniques he designed two probes. First he replaced a sector of a (TEM) bulk specimen carrier with a 200-mesh nickel screen (see fig.1). The grid material is coated with a carbon or silicon oxide film by evaporative deposition after being bonded to the modified carrier. However this probe is fragile and more difficult to fabricate and coat uniformly because of the large grid surface. A second probe consists of a carrier through which a slot has been milled (see fig.2). Conventional coated grids are bonded to the carrier with epoxy cement to provide a durable and more easily constructed probe. This probe has a larger thermal inertia, is inexpensively fabricated from the commercially available carbon-coated circular grids and the bulk specimen carrier, and is highly durable. Dobbins found this to be the most advantageous probe.

He measured the temperature of his probes by means of temperature-indicating liquids, in a flame of 1900 K the probe temperature rises to $385 \pm 10$ K in a sampling time of 65 ms. The grid temperature he expects to be substantially higher since this has a lower thermal inertia. He derived formulas for deposition and quenching times, these formulas are given in the last chapter.

### 3.1.2 Pendulum.

Stefanović [Lit. 10] used an uncooled flying Pitot-tube to measure the stagnation pressure distribution in a high temperature free fluid flow. In principle a pendulum might be suited to sample particles from the flame since it renders short residence times, it is easy to operate and relatively cheap. An accurate mathematical model yields straightforward the velocity and the trajectory.

### 3.1.3 Thermocouple response technique

Eisner [Lit.11] shows that, because of the dominance of thermophoresis, the transient response of a fine thermocouple inserted into a soot laden combustion gas mixture can be used not only to infer local gas temperatures, but may also be used to estimate local soot volume fractions, without having to make rather restrictive assumptions about the prevailing particle size distribution or particle optical properties. Due to thermophoretic deposition on the thermocouple the diameter of the wire will change. In principle the particle flux is dependent of the number concentration of the particles in the gas (see equation (26)). So by measuring the thickness of the deposited layer it is possible to deduct the particle concentration. He presents two variants of this procedure, one of which is based on his direct measurements of the time-dependence of the TC-bead diameter, while temperature is also recorded. The second procedure which involves simultaneous use of a quasi-static energy balance on the TC-bead, only requires measurement of the TC-bead $T_w(t)$-relation where $T_w$ is the temperature of the wall of the TC-bead.

## 3.2 Molecular beam sampling.

An aerosol beam/ molecular beam is generated when an aerosol or gas expands through an orifice, capillary, or nozzle into an evacuated chamber. The gaseous portion of the jet is scattered by collisions with background gas molecules and removed by pumping. The particles or droplets in the aerosol, are not scattered by background gas, because of their relatively large momentum, but form a high speed beam of aerosol particles. The aerosol particles are thus isolated from their suspending gas.
The cross-section of an aerosol beam always grows with downbeam displacement in the chamber. The beam divergence is of course caused by radial expansion of the aerosol jet as it enters the vacuum chamber. To reduce the width of the beam it is often skimmed.
Most authors use Fristrom [Lit.12] as a reference for the design of their probes. According to Fristrom a probe should be designed in such a way that it produces a minimum disturbance in the flame. This disturbance arises both from sample withdrawal and from the bulk of the probe itself. A probe must also allow a pressure drop to freeze the reactions, and withdrawal of the sample to a cool region outside the flame. These objectives can be accomplished by use of a tapered quartz microprobe with a small sonic orifice

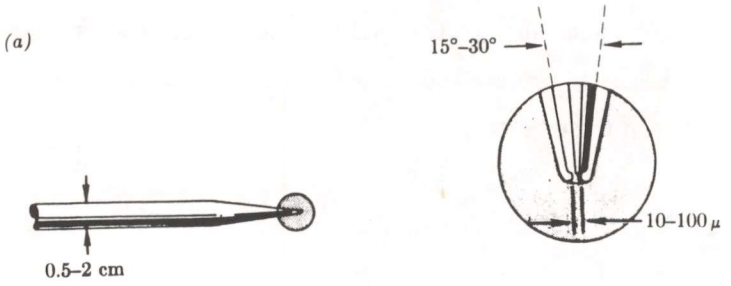


Fig. 3 Molecular beam probe with its typical dimensions

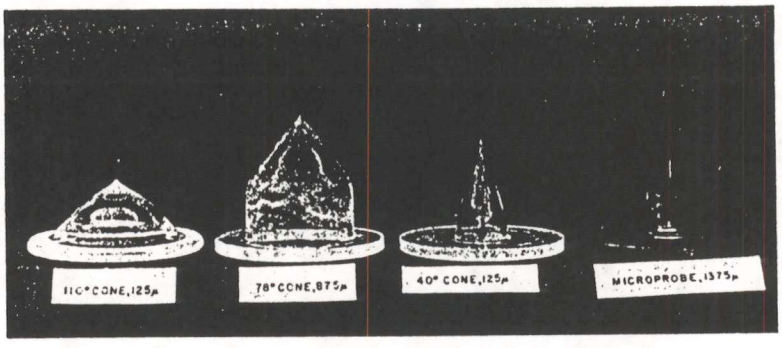


(a)


(b)

Fig. 4 (a). Example of four types of quartz probes used to examine flame structure and perturbation. The last number on the labels is the orifice diameter in micrometers. The diameter of the disc, which forms the base of the probe in each case, is 6.8 cm and its thickness is 0.48 cm. (b) Examples of "hybrid" probes. The dimensions of the base are as in (a).

inlet (see fig.3). He advises to design the probe in such a way that there is a five to tenfold pressure drop over the orifice.

The quenching of a chemical reaction is the most important requirement of a probe if it is to provide a meaningful sample. In a critical flow probe, which is the only type with any hope of rapid enough quenching, this is accomplished by the drop in pressure and temperature accompanying expansion of the gas as it flows through the probe. It can be seen intuitively that, if the temperature and pressure drop rapidly, compared with the reaction times, the sample will be quenched or frozen. According to Fristrom [Lit.12 p193] the input pressure is crucial, the lower it is the quicker the sample is quenched. According to Fristrom a lot of work has been done on the flow of reacting gases in supersonic nozzles for rockets and windtunnels. These numerical calculations show that the temperature dropped 1500 K within 50 $\mu$s and the concentration values of the major components are within a few percent of their input values, only radicals show larger deviations. While no studies have been performed on sampling probes with very small nozzles he expects them to perform well since the small dimensions mean short residence times to reach a certain area ratio which is the most important parameter in quenching. Seery [Lit.13] thinks for good quenching capability it is necessary to have a pressure drop over the orifice of a factor $10^5$.

In the area of combustion technology molecular beam sampling (MBS) is a widely used technique. MBS is used in two different set ups. In the first case it is used to deposit material on a TEM grid. In the other case the MB-probe is directly coupled to a mass-spectrometer. An example of a MB-probes is shown in fig.4. MB systems usually extract a small portion of the sample jet originating at the probe orifice by means of a skimmer. This is then passed to the TEM-grid or the mass-spectrometer for analysis. In a typical configuration this consists of the central 2.5% (by volume) of the jet. Most probes used in literature have cone angles between 40 and 60 ° [Lit. 14, 15]. Orifice diameters vary from several $\mu$m to 1 mm [See lit.,16,17,18] The upper value of the orifice diameter is limited by the pumping capacity. The pressure is reduced over the first cone by a factor $10^3$ to $10^5$ and by a factor 100 over the skimmer , the length of the cones is about 5 cm.

### 3.2.1 MBS for the Electron microscope.

Bockhorn e.a. [lit.14] used MB sampling for the electron microscope. He used a 50 mm long probe with an orifice of 450 $\mu$ and an angle of 60 ° . For the microscope he used round copper nets with a diameter of 3 mm, mesh number 200 coated with 8-10 nm carbon and slit them into the beam 130 mm from the tip of the cone for 2-45 s. Dahneke [Lit.19] measured the capture limit velocity, of latex spheres (d 1.27$\mu$), above which bouncing predominated and below which sticking occurred. The velocity he found was in the order of 1 m/s on a polished surface. He suggests to take softer material to deposit on. Bockhorn does not mention this phenomena of particle bouncing and probably assumes all particles to stick.

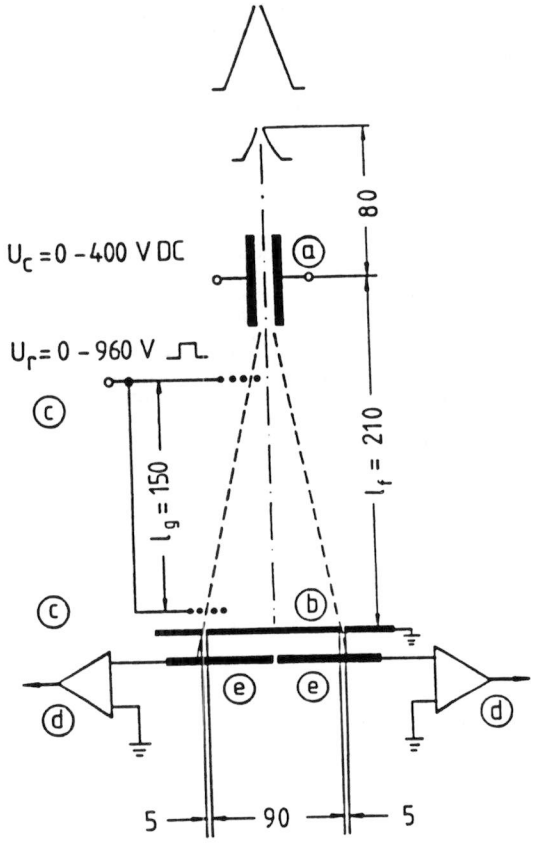


FIG. 5 Particle kinetic energy and particle velocity analysers: a) capacitor, b) blend, c) grid, d) amplifier, e) electrode.

### 3.2.2 MBS coupled to a mass-spectrometer.

In literature many applications of molecular beam coupled to a mass spectrometer (MBMS) are reported. Korobeinichev [Lit.17] names the following advantages : it provides component identification, position determination and concentration distribution with a high spatial resolution compared to spectroscopic methods. Korobeinichev uses a silica or metal cone with a 100 $\mu$ hole and feeds the molecular beam to a time of flight mass spectrometer. The beam is passed to an ion source and modulated by a chopper to correct for scattered background. The expected error is less than 10 %.

Smyth [Lit.16] like most authors feeds the molecular beam directly into the ionization chamber of a quadrupole mass spectrometer. He used a 6 mm outer diameter quartz tube tapered to a tip with an orifice diameter of 140 $\mu$m. The pressure downstream from the probe was typically 13-40 Pa this means a pressure ratio over the orifice of 2500. He measured profiles of the major species present in a flame.

Biordi [Lit.20] chopped the beam too before it was fed to the quadrupole MS and used several different probes for determining the concentrations. The orifice size he used was limited by pumping capacity to 140 $\mu$ but was more often between 75 and 125 $\mu$. The wall thickness varied between 50 and 125 $\mu$. Some of the probes he used are displayed in fig 4. Seery [Lit. 13] measured the profile of NO in a flame.

Stepowski [Lit.21] measured the OH-profile in a flame using a MBMS system. He used a system with 3 differentially pumped stages, the first one equipped with a conical thin wall deactivated quartz sampling probe, 65 mm high, with an external angle of 40 ° and a 100 $\mu$m diameter orifice. He used Laser Induced Fluorescence to verify the agreement between the two techniques. This agreement he found to be very good if he measured outside the very reactive zone of the flame.

### 3.2.3 Measurements of kinetic energy and charge using MB-sampling.

Hospital [lit.22, 23] used the system drawn in fig.5 to measure charge and kinetic energy of particles in a flame. His apparatus, he thinks, fills the gap between mass-spectrometry and electron microscopy. He used a probe with a 0.76 mm diameter platina plated and electrically grounded 45° quartz nozzle. Over the nozzle the pressure was reduced from 20 mbar to $10^{-3}$ mbar ( a factor $2*10^4$ !) The centre of the jet was extracted through a 0.69 mm diameter skimmer into a chamber were the pressure was maintained at $10^{-5}$ mbar. The distance between nozzle and skimmer was 76 mm which causes not only a low density but a small divergence as well.

The charged particles are deflected due to the electric field in the capacitor. The deflection is given by :

$$d = \frac{n_e \cdot e}{m_p \cdot v_p^2} \cdot \frac{U_c \cdot l_c \cdot l_f}{b_c} \qquad (10)$$

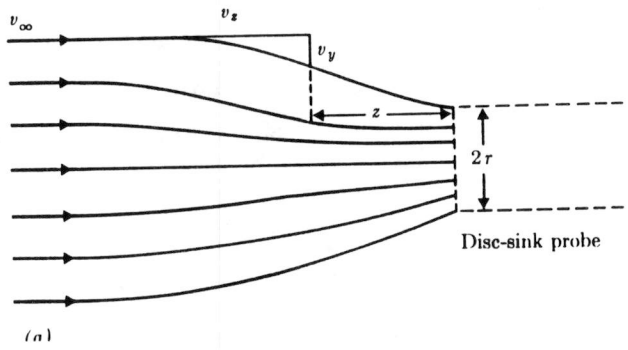


Fig. 6 Disk-sink probe with its dimensions

which is easily derived from basic principles. The first group in this formula has the character of a inverse kinetic energy E per charge:

$$E = \frac{m_p \cdot v_p^2}{n_e \cdot e} \tag{11}$$

Introducing this in to formula (5) gives :

$$U_c = E \cdot d \cdot \frac{b_c}{l_c \cdot l_f} \tag{12}$$

Now it can be seen that under fixed geometrical conditions (i.e. $d, l_f, l_c$ ), with increasing voltage particles with increasing energy are registered at the electrodes. Adding a pulse voltage at electrode C it is possible to select particles with a certain velocity to reach the electrodes. Now in combination with the measured kinetic energy it is possible to determine the mass from equation 8.

### 3.4 Perturbation of the flame by the probe

The important questions to be considered in the present context can be grouped together under the general problem of interpretation , i.e., the degree in which the measured sample composition corresponds to the actual composition in the unperturbed flame at the position determined. The various perturbing effects may now be assessed individually.

#### 3.4.1 Aerodynamic effects.

Aerodynamic flow in a flame is disturbed both by the wake of the probe and by the fact that there is a sample withdrawal. Fristrom thinks these effects tend to cancel. The distortion introduced by sample withdrawal alone has been discussed theoretically by Rosen [Lit.24], using a disk sink model. In the incompressible flow approximation , the approach flow lines into the sink were calculated. Refer to fig.6; a sink of radius r and strength ( volumetric flow rate) $\Phi_v$ distorts the unperturbed velocity $v_\infty$, as shown schematically. According to Fristrom the theoretical treatment gave an expression for the fractional flow distortion $v_y/v_\infty$ as a function of the distance z and the sampling ratio $\alpha$:

$$\alpha = \frac{\Phi_v}{\pi \cdot r^2 \cdot v_\infty} \tag{13}$$

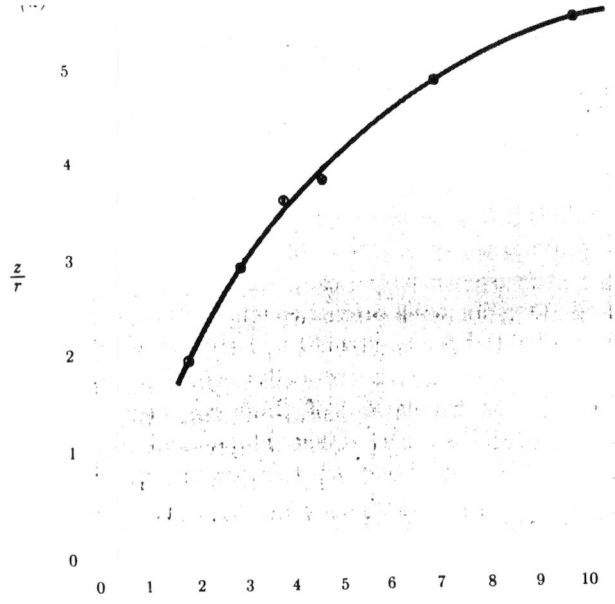


*(b)*

**Fig. 7** Theoretical calculation of incompressible flow into a disk-sink probe [14]. (*a*) Schematic of flow lines showing distortion due to sink. (*b*) Distance (number of sink radii) ahead of probe at which distortion $v_y/v_\infty$ is 5%, as function of sampling rate ratio $\alpha$ ($= Q/\pi r^2 v_\infty$, where $Q$ is volumetric flow into sink).

Fig.7 shows the result for a flow distortion of $v_y/v_\infty$ = 5 percent. Typical probe sampling rates correspond to values of $\alpha$ in the range 10 to 100, so that a 5 percent distortion would be estimated to occur 5 to 10 probe radii(z/r) upstream. For a probe with r= 10$\mu$ this distance would be 0.05 to 0.1 mm, which is not a serious aerodynamic disturbance.

### 3.4.2 Concentration effects.

A more subtle question than the foregoing strictly aerodynamic problem is this: does a probe sample the composition of a gas at a point, the sum of the fluxes of the various gases through the sampled cross-section, or something different of either of these? Since the flame is characterized by steep concentration gradients, the flow perturbation set up by the sample withdrawal would be expected to alter the original gradients and thus the composition of the gas entering the probe. In MBMS sampling, probe distortions have been observed by several investigators. Biordi et al. [lit.20] measured concentration profiles in flames at 0.04 atm; the methane concentration profile measured by MBMS using a 20 ° half angle sampling probe appeared to be shifted about 5 orifice diameters relative to that measured using a microprobe. Stepowski [lit.21] measured OH profiles in flames at 0.033 atm; The profile measured by MBMS appeared to be shifted about two orifice diameters relative to that measured using laser induced fluorescence. Cattolica [lit.25] measured OH and temperature profiles in flames at 1 atm; the OH profile measured by MBMS appeared to be shifted about 5 orifice diameters relative to that measured by laser absorption spectroscopy, and the temperature profile measured by MBMS also appeared to be shifted about 5 orifice diameters relative to that measured using a thermocouple. These measurements suggest that the MBMS samples are from a location upstream from the probe tip, the distance from the probe tip to the sampling location depending on the probe-orifice diameter and other system parameters yet to be identified. Yi and Knuth [lit 26] made an analysis for an infinite long conical probe, with circular orifice at the tip, located in a binary-mixture stream containing a concentration gradient and a first order reaction. Far upstream from the probe the flow is parallel to the cone axis and toward the cone. In the vicinity of the cone the flow is axisymmetric, laminar and compressible. At the plane of the orifice the flow is sonic. They examined the perturbations for different combinations of the product of Re and Sc:

$$Re \cdot Sc = \frac{v_\infty \cdot d_\infty}{D} \qquad (14)$$

Where v stands for velocity $d_c$ the diameter of the cone and D is the diffusion coefficient, and of the dimensionless group $\Pi_1$ :

$$\Pi_1 = \frac{d_\infty}{v_o \cdot \tau_r} \qquad (15)$$

where $v_0$ is the velocity of the gas at the orifice inlet, $\tau_r$ is the characteristic reaction time.
For $(Re \cdot Sc) \gg 1$ they found that the shift of the measured concentration profile $\delta$ is given by :

$$\frac{\delta}{d_{co}} = 0.19 \cdot (Re \cdot Sc)^{1/4} \qquad (16)$$

In this equation the influence of $\Pi_1$ is neglected since the influence of this group is negligible compared to the influence of $(Re \cdot Sc)^{1/2}$.

### 3.4.3 Thermal effects.

A probe represents a heat sink which can disturb the flame by reducing temperature and enthalpy in the region being sampled. According to Fristrom with an uncooled quartz probe, radiation is the primary heat loss mechanism. Quartz has a very low emissivity ($\epsilon \approx 0.02$), and at 2000 K at the tip, rough calculations indicate that less than 1 percent of the sample enthalpy would be extracted prior to sampling. This would lower the temperature by less than 20 K. Since this effect varies as $T^4$ it would be less than 1 K at 1000 K and negligible below this point.

### 3.4.4 Catalytic effects.

Within the combustion area a probe might perturb the flame in terms of heterogenic catalytic effects, in our application I do not think it is necessary to discuss this problem.

### 3.4.5 Summary

MB can be a suitable sampling system though several problems have to be solved. One of the major problems I expect is clogging of the orifice since the particle concentration is quite high.
Many authors use low pressure flames which enables them to create large pressure drops with relatively small pumps and in this way create good quenching capability. And low pressure itself favours rapid quenching.
Correction for sampling location is a problem since the theories developed have only corrections for reactions with relaxation times of $1*10^{-3}$ and $7*10^{-4}$ s. Furthermore I expect the errors due to the introduction of the probe into the flame to be much greater since the flame we use is much smaller than the flames used in literature.
Errors can be expected due to the expansion of the gas (small particles follow the streamlines better than the large ones) and perturbation of the flame by the probe.

When MB-sampling is used to deposit material for analysis in a TEM errors due to particle bouncing will be very small since small particles will show great tendency to stick.

Two of the major advantages are

- the known volume which is sampled, it is restricted to several cubic mm, while the volume sampled using thermophoretic deposition is larger and unknown.
- due to the pressure drop the reactions are effectively frozen.

In first instance I would recommend thermophoretic sampling since it is rather simple, this simplicity is the major problem in this technique as well since the sample volume and place are rather difficult to determine.

## 4 Other techniques

### 4.1 Differential Mobility analyzer.

Within the aerosol world the differential mobility analyzer (DMA) is often used. Okuyama [Lit. 27] and Flagan [Lit.28] used a DMA to determine the psd of $TiO_2$ formed during a gas phase reaction. Van Dingenen [Lit.29] used a DMA to determine the size of $H_2SO_4$ aerosol formed by the oxidation of $SO_2$. The DMA consists of two concentric cylinders. Particles enter the analyzer through a slot in the outer cylinder wall, and are deflected toward the inner cylinder by an imposed electric field. The flowrate of the aerosol is $\Phi_a$. A sheath air flow, $\Phi_{sh}$, initially separates the aerosol from the collection rod. A sample flow $\Phi_s$, is extracted through a slot around the collection rod.The collection rod is maintained at a voltage V. Only particles with mobilities within a limited range will enter the sample stream for detection. By examining limiting trajectories of particles at various points in the aerosol flow in the entrance to the analyzer column, Knutson and Whitby [Lit.30] showed that the fraction of the particles that will be extracted for measurement is :

$$\Omega = \max\left[0, \min\left(\left[1, \frac{\Phi_s - \Phi_{sh} + K}{\Phi_a}, \frac{\Phi_a + \Phi_{sh} - K}{\Phi_a}, \frac{\Phi_s}{\Phi_a}\right]\right)\right] \qquad (17)$$

Where

$$K = -2 \cdot \pi \cdot r_1 \cdot E_1 \cdot Z_p \cdot L \qquad (18)$$

$r_1$ is the radius of the collection rod, $E_1$ is the electric field at the rod surface, $Z_p$ is the mobility of the particle and $\Omega$ is called the instrument transfer function. To measure a particle size distribution with a DMA, the collector rod voltage is set to give the desired value of K, and the number concentration in the range of mobilities transmitted through the sample extraction slot is measured with an electrometer or a condensation nucleus counter after the signal reaches a steady value. The collection rod voltage is then stepped to a new level and the measurement is repeated. The time required to acquire a complete particle size distribution, according to Flagan, depends on the number of size intervals to be measured, the time for the particles to pass through the analyzer column, and the settling averaging times for the detector. Typically 10 to 20 seconds are allowed per size interval measured. Thus, determination of the concentration at one size may require 10 to 30 seconds. Measurement of a 100 interval size distribution thus requires 15 to 50 minutes. The charge distribution on the aerosol is first allowed to approach a steady-state bipolar charge distribution by passing the aerosol through a bipolar diffusion charger. The accuracy of this instrument depends on the accuracy of the flow rates and the voltage used. The sheath gas and excess gasflow are connected in a recirculating flow to ensure accurate dilution ratios.

4.2 Scanning Electrical Mobility Spectrometer

Wang and Flagan [Lit.31, 32] describe a DMA where the collector rod voltage $E_1$ is allowed to vary continuously, they call this DMA a Scanning Electrical Mobility Spectrometer (SEMS). The fraction of the particles of mobility $Z_p$ that will enter the sample flow is given by the following transfer function:

$$\Omega = \max\left[0, \min\left(\frac{K(t_m) + \Phi_s - \Phi_{sh}}{\Phi_a}, \frac{-K(t_m) + \Phi_a + \Phi_{sh}}{\Phi_a}, \frac{\Phi_s}{\Phi_a}, 1\right)\right] \quad (19)$$

Equation 16 is identical to equation 15 except for the way the mobility parameter K is defined. If the electric field is ramped exponentially with time (either up or down):

$$E_1(t) = \beta e^{\pm\frac{t}{\tau}} \quad (20)$$

the value of $K(t_m)$ is given by

$$K(t_m) = \mp 2 \cdot \pi \cdot r_1 \cdot Z_p \cdot L \cdot \frac{\beta \cdot \tau}{t_f}\left[1 - e^{\mp\frac{t_f}{\tau}}\right] \times e^{\pm\frac{t_m}{\tau}} \quad (21)$$

where $t_f$ is the residence time in the analyzer column.

Wang thinks it is possible for the transfer function to differ from the one given in eq. 13 due to nonuniform electric fields or gas velocities but at least it will be the same for all mobilities. This way the size distribution can be measured by continuously changing the analyzer voltage and continuously monitoring the concentration of particles leaving in the sample stream. This mode of operation can greatly accelerate the measurement of size distribution since it is no longer necessary to wait for the particles in the analyzer column or in the plumbing between the analyzer and detector, or to wait for the detector itself to achieve a new steady state. Moreover because the voltage in the analyzer column is changed slowly, the electronic settling time of the analyzer does not impede data acquisition.

The SEMS was demonstrated by Wang and Flagan, in their setup the collector rod voltage is varied by means of an IBM/AT, the software used was written in turbo pascal. They measured a complete size distribution (10-100 nm) in 30 seconds. To measure the same size distribution with a DMA in the stepping mode would have taken 7 minutes. The agreement between the two measurements is fairly good, the main problems arise in the lower size classes due to low charging efficiencies.

4.3 Diffusion battery.

Diffusion batteries are devices that separate particles according to their diffusion coefficients, based on relationships for diffusion losses from laminar flow. They are used to measure aerosol diffusion coefficients

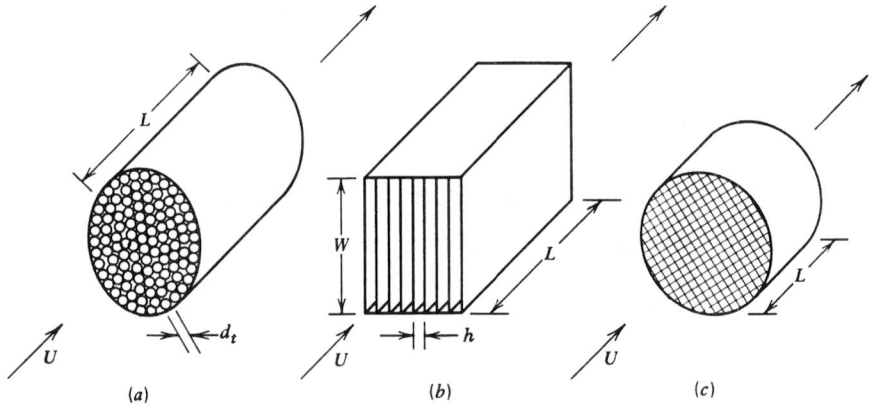


**Figure 8 Three types of diffusion batteries. (*a*) Tube bundle. (*b*) Parallel plate or rectangular channel. (*c*) Screen type.**

by measuring the concentration of particles entering and leaving a tube or similar conduit. The average value of the dimensionless deposition parameter $\mu$

$$\mu = \frac{D \cdot L}{\Phi_v} \tag{22}$$

where $\Phi_v$ is the volumetric flowrate L the length of the tube and D the diffusion coefficient of the particle. and the diffusion coefficient of the aerosol flowing through the tube are obtained by inverse application of:

$$P = \frac{N_{out}}{N_{in}} = 1 - 5.50\mu^{2/3} + 3.77\mu \qquad \text{for } \mu < 0.007 \tag{23}$$

$$P = 0.819\exp(-11.5\mu) + 0.0975\exp(-70.1\mu) + 0.0325\exp(-179\mu) \qquad \text{for } \mu > 0.007 \tag{24}$$

These formulas give the penetration P for a tube bundle diffusion battery (See fig.8). For a parallel plate diffusion battery, which is simpler to construct and often more compact than the equivalent tube bundle type, slightly different equations must be used. The third type of diffusion battery uses multiple layers of very fine mesh wire cloth. The flow through the gaps in the weave is equivalent to flow through a large numbers of small pores similar to the tube bundles described above. The mechanism of collection is different of that from that of a tube and the penetration is given by Cheng[Lit.33]:

$$P = \frac{n_{out}}{n_{in}} = \exp\left(\frac{-10.8\epsilon L D^{2/3}}{\pi(1-\epsilon) d_w^{5/3} v^{2/3}}\right) \tag{25}$$

Where $1-\epsilon$ is screen porosity, $d_w$ is the wire diameter, v is the velocity and L is the depth of the holes. Knutson [lit.34] used diffusion batteries which enabled him to determine the particle size distribution of radioactive aerosols in the size range from 2 to 500 nm. He made an intercomparison between three diffusion batteries, two screen type diffusion batteries and one disc-type battery. He differentiates between a major and a minor mode, the major mode is a very large amount of particles in the 150 nm region, the minor mode is a smaller amount of particles in the region smaller than 10 nm. For the major mode he found the agreement between the three good unless there was a substantial amount of particles present which were larger than 500 nm. For the minor mode the three batteries frequently disagreed on the existence, location and amplitude.

## 4.4 Summary

All three techniques are fitted for our application though non of them is capable of giving direct information about the processes taking place in the flame. A major advantage of the DMA is its availability to us. Though

the SEMS is a great improvement of the DMA the time required to build and calibrate is an uncertainty. The diffusion battery seems a good apparatus as well if a complete set is available, that is, including the deconvolution algorithms. Combining the results of the DMA and of a diffusion battery could render some new insights in the process. All three systems probably need dilution first which might alter the size distribution.

## 5.Thermophoresis.

When a temperature gradient is established in a gas, the aerosol particles in the gas experience a force in the direction of decreasing temperature. The motion of the aerosol particle that results from this force is called thermophoresis. The magnitude of the thermal force depends on gas and particle properties and the temperature gradient. The earliest studies of thermophoresis were empirical studies of the dust-free layer around a heated object, such as a metal rod immersed in smoke. Measurements of the thickness of this layer established that it is independent of smoke material and proportional to the square root of the temperature difference between the object and the gas. When cold surfaces are proximate to a warm gas thermophoresis causes particles to be deposited on the cold surfaces.

For small particles, $d_p$ smaller than the mean free path of the gas, the thermal force is a result of greater momentum transfer from the gas molecules on the hot side of the particles compared to the cold side. This greater momentum causes a net force , the thermal force, in the direction of the cooler temperature. The velocity of thermophoresis, $V_{th}$, is given by Waltmann and Schmitt [lit.35] as :

$$V_{th} = \frac{-0.55 \cdot \eta \cdot \nabla T}{\rho_g \cdot T_p} \qquad (26)$$

Where $\eta$ is the viscosity of the gas, $\rho_g$ the density of the gas, $T_p$ the temperature of the particle and $\nabla T$ the temperature gradient. As can be seen from this formula the thermophoretic velocity is independent of the particle size and directly proportional to the temperature gradient.

For particle sizes equal or larger than the mean free path of the gas the formulas get much more complicated and there is still discussion on what formula to use in which case.

### 4.1 Deposition on a probe.

The probe exposure time should be long enough to capture a significant sample but short enough to present a cold surface to the flame-born particles. This cold surface serves a second important purpose which is that it freezes heterogenous reactions of the particles that are already captured. This chemical freezing prevents changes in particle morphology after the particles have impacted on the cold surface. The theoretical description of the thermophoretic transport of particles is provided by the analysis of the particle drift across a thermal boundary layer formed over a solid surface in a particle-laden, hot gas stream. The heat flow from the gas to the surface of the probe is given by:

$$\Phi''_h = -h \cdot \Delta T \qquad (27)$$

where h is the heat transfer coefficient ($W/m^2 \cdot K$). The heat flux through the boundary layer is given by:

$$\Phi''_h = -\lambda_g \cdot \nabla T \tag{28}$$

where $\lambda$ is the heat conductivity of the gas ($W/m \cdot K$).

When the number density of the particles in the gas is given by $N_p$, the particle flux $J_w''$ per unit area is given by velocity times number density:

$$-J''_w = \frac{k_{th} \cdot \eta_g \cdot \nabla T \cdot N_p}{\rho_g \cdot T_p} \tag{29}$$

In the thermal boundary layer energy and particle mass are each conserved. For heat transport this implies:

$$\nabla T = \frac{h}{\lambda_g} \cdot \Delta T \tag{30}$$

Substitution in (26) yields:

$$-J''_w = \frac{k_{th} \eta_g N_p}{\rho_g} \cdot \frac{h}{\lambda_g} \cdot \frac{\Delta T}{T_p} \tag{31}$$

introducing the boundary layer thickness $\delta_t$ yields:

$$-J''_w = \frac{k_{th} \eta_g N_p}{\rho_g} \cdot \frac{(Nu)_{cp}}{\delta_t} \cdot \frac{\Delta T}{T_p} \tag{32}$$

In the thermal boundary layer the temperature drops from the gas temperature $T_g$ to the temperature of the wall of the probe $T_w$ at the wall of the probe. Correcting for the temperature dependence of $\lambda_g$ and assuming the temperature of the particle to be equal to the gas temperature $T_g$ yields:

$$-J''_w = \frac{k_{th} \eta_g N_p}{\rho_g} \left[\frac{T_w}{T_g}\right]^{\kappa} \left[1 - \frac{T_w}{T_g}\right] \cdot \frac{Nu}{\delta_t} \tag{33}$$

When Nu=0 this is the formula used by Dobbins [Lit.9] in his paper. For the derivation of this formula he refers to Eisner [Lit.11] but Eisners formula looks slightly different, instead of the thickness of the boundary layer he uses the diameter of his (round) thermocouple:

$$-J''_w = \frac{k_{th} \eta_g N_p}{\rho_g} \cdot \frac{(Nu)_{cp}}{d_w} \cdot \frac{1}{1+\kappa} \left[1 - \left(\frac{T_w}{T_g}\right)^{1+\kappa}\right] \tag{34}$$

Eisner in his article does not assume Nu to be 0.

From formula (30) Dobbins estimates the exposure time for 10 % coverage of the surface to be:

$$\tau_e = \frac{0.4}{\pi J''_w d_p^2} \tag{35}$$

He defines the quench time as follows: the time needed by the particle to traverse from the hot flame gases to the cold surface of the probe. In equation (26) he then makes the following approximation:

$$\frac{\rho_g}{\eta_g} \cdot \frac{\nabla T}{T} \sim \nu_a \frac{T_w - T_g}{\delta_t T_a} \tag{36}$$

where $T_a$ is the average temperature of the layer and $\nu_a$ is the kinematic viscosity of the gas at $T_a$. The quench time $\tau_q$ is then given by:

$$\tau_q = \frac{T_a \delta_t^2}{k_{th} \nu_a [T_g - T_w]} \tag{37}$$

## 6. Conclusions

The aim of this literature search was to investigate the possible particle size analysis techniques. These techniques were divided in three groups. The first group consists of techniques which make use of some sort of light to determine the particle size in-situ without disturbing the processes taking place in the reaction zone. In theory these techniques are therefore the ideal techniques, but they all require specialists to guarantee reliable results. Most of the techniques require knowledge of the particle refractive index which is a function of the chemical composition. Furthermore the time required to implement these systems in our experimental setup is most probably too long.

The second group of techniques consists of techniques which sample directly in the reaction zone, therefore they are likely to influence the results. Molecular beam sampling though it has many applications within the combustion science is not so suitable since the dimensions of our flame (diameter $\approx$ 1 cm) are small compared to the dimensions of the flames used in literature (width $\approx$ 15 cm). I therefore expect the errors introduced by the probe to be much bigger than acceptable.

The pendulum is not possible because of lack of space in the reactor. The method of Dobbins I think is the most promising in this group since it yields control over sampling time and place, and the construction is relatively easy.

The last group of techniques only yield information of particle size at the end of the reactor but the information extracted from these methods on the influence of parameters as gasflow and laser power on product properties could be really valuable. Both DMA and diffusion battery are fitted for our application the major advantage of the DMA is its availability to us.

**Literature**


1. E.J. Jacquemijns, P.J. van der Put, J. Schoonman, Vapour phase synthesis of ultrafine silicon nitride powders., High temperatures-high pressures, **20**, pp. 31-34 (1988).

2. W.R. Cannon, S.C. Danforth, J.S. Haggerty, R.A. Marra, Sinterable ceramic powders from laser driven reactions:II, Powder chracteristics and process variables., J.Am.Ceram.Soc., **65**, pp. 330-335(1982)

3. J.S. Haggerty, Sinterable ceramic powders from laser heated gas phase reactions and rapidly solidified ceramic materials. Report MIT-EL 84-009 (1984).

4. R.J. Santoro, H.G. Semerjian, R.A. Dobbins, Soot particle measurements in diffusion flames, Comb. and flame **51**, pp. 203-218 (1983).

5. P. Gougeon, J.N. Le Toulouzan, C. Thenard, G. Gouesbet, Simultaneous measurements of sizes and concentrations of coal particles in multiple scattering media by means of a double extinction technique., Particle size analysis 1985, pp.383-393. ed. P.J. Lloyd

6. J.F. Driscoll, D.M. Mann, W.K. McGregor, Submicron particle size measurements in an acetylene-oxygene flame., Combustion Science and Technology, **20**, pp. 41-47 (1979).

7. T. Ohsawa, E. Kobayashi, T. Ozaki, FFT Method of dynamic light scattering for particle size diagnostics in luminous flames., Combustion and Flame **53**, pp. 135-139 (1983).

8. A. Cavaliere, R. Ragucci, A. d'Allessio, C. Noviello, Analysis of diesel sprays through two-dimensional laser light scattering., Twenty-Second Symposium (International) on Combustion, the Combustion Institute, pp.1973-1981 (1988).

9. R.A. Dobbins, C.M. Megaridis, Morphology of flame-generated soot as determined by thermophoretic sampling., Langmuir, **3**, 2, pp. 254-259 (1987).

11. A.D. Eisner, D.E. Rosner, Experimental studies of soot particle thermophoresis in non isothermal combustion gases using thermocouple response techniques., Comb. flame, **61**, pp. 153-166 (1985).

10. P. Stefanović, S. Oka, P. Pavlović, J. Jovanović, M. Matović, Stagnation pressure measurement in high temperature jet flow using flying Pitot-probe., Measurement techniques in heat and mass transfer., ed. R.I. Soloukhin, N.H. Afgan, Hemisphere Publ. Corp. Washington (1985).

12. R.M. Fristrom, A.A. Westenberg, Flame structure., McGraw-Hill 1965.

13. D.J. Seery, M.F. Zabielski, Comparisons between Flame species measured by probe sampling and optical spectrometry techniques., Comb. Flame, **78**, pp. 169-177 (1989).

14. R.A. Bockhorn, Twenty-first Symposium (International) on Combustion, the Combustion Institute, pp.1001 (1986).

15. O.I. Smith, D.W. Chandler, An experimental study of probe distortions to the structure of one dimensional flames., Comb. Flame, **63**, pp. 19-29 (1986).

16. K.C. Smyth, J.H. Miller, R.C. Dorfman, W.G. Mallard, R.J. Santoro, Soot inception in a methane/air diffusion flame as characterized by detailed species profiles., Comb. flame, **62**, pp.157-181 (1985).

17. O.P. Korobeinichev, A.G. Tereshchenko, I.D. Emel'yanov, A.L. Rudnitskii, S.Yu. Fedorov, L.V. Kuibida, V.V. Lotov, Substantation of the mass-spectrometric method for studying the structure offlames with narrow combustion zones., Fizika Goreniya i Vzryva, **21**, 5, pp. 22-28 (1985).

18. O.P. Korobeinichev, Dynamic flame probe mass spectrometry and condensed-system decomposition., Fizika Goreniya i Vzryva, **23**, 5, pp. 64-76 (1987).

19. Dahneke, J. of Coll. Sci. **45**, 3, pp. 584-590 (1973).

20. J.C. Biordi. C.P. Lazzara, J.F. Papp, Molecular beam mass spectrometry applied to determining the kinetics of reactions in flames. I. Empirical characterization of flame perturberation by molecular beam sampling probes., Comb. Falme, **23**, pp. 73-82 (1974).

21. D. Stepowski, D. Puechberty, M.J. Cottereau, Use of laser induced fluorescence of Oh to study the perturberation of a flame by a probe., Eighteenth Symposium (International) on Combustion, the Combustion Institute, pp.1567-1573 (1981).

22. A. Hospital, P. Roth, In-situ mass growth measurements of charged soot particles from low pressure flames., Twenty-third Symposium (International) on Combustion, the Combustion Institute, pp.1573-1579 (1990).

23. A. Hospital, P. Roth, J. aerosol. Sci., **21(supl.1)**, pp. s35-s38 (19??).

24. P. Rosen, Potential flow of a liquid into a sampling probe, Johns Hopkins Univ. Appl. Phys. Lab. Rept. CF-2248, Silver Spring, Md. (1954)

25. R.J. Cattolica, S. Yoon, E.L. Knuth, Comb. Sci. and Tech., **28**, p.225 (1982).

26. A.C. Yi, E.L. Knuth, Probe-induced concentration distortions in molecular-beam mass-spectrometer sampling., Comb. flame, **63** ,pp. 369-379 (1986).

27. K. Okuyama, Y. Kousaka, N. Tohge, S. Yamamoto, J. Jwang, R.C. Flagan, J.H. Seinfeld, Production of ultrafine metal oxide particles by thermal decomposition of metal alkoxide vapors., AIChE Journal, **32**, 12, pp. 2010-2019 (1986).

28. R.C. Flagan, S.N. Rogak, Fundamenal studies of particle growth and structure during powder synthesis, International fine particle research institute ARR 20-01 (1990).

29. R. van Dingenen, F. Raes, The dynamics of sub-micron $H_2O$-$H_2SO_4$ aerosols: a smog chamber study., third international aerosol conference (1990).

30. K.T. Whitby, E.O. Knutson, J. Aerosol. Sci., **6**, p.443 (1975).

31. S.W. Wang, R.C. Flagan, Scanning electrical mobility spectrometer, J. Aerosol. Sci., **20**, 8, pp. 1485-1488 (1989).

32. S.W. Wang, R.C. Flagan, Scanning electrical mobility spectrometer, Aerosol. Sci. tech.

33. Y.S. Cheng, H.C. Yeh, J.Aerosol. Sci., **11**, pp. 313-320 (1980).

34. E.O. Knutson, K.W. Tu, S.B. Solomon, J. Strong, Intercomparison of three diffusion batteries for the measurment of radon decay product particle size distributions., Radiation Protection Dosimetry, **24**, 1/4, pp. 261-264(1988).

35. L. Waldmann, K.H. Schmitt, Aerosol Science, ed. C.N. Davies, Academic press, London (1966).

36. D.W. Mackowski, R.A. Altenkirch, M.P. Menguc, Multiple-wavelength pyrometer measurement of particle size in pulverized-coal flames., Chemical and physical processes in combustion, paper 52, Fall technical meeting eastern section of the Combustion Institute (1985).

**Symbols.**

| | | |
|---|---|---|
| C | slip-correction factor | [-] |
| $b_c$ | width of the capacitor | [m] |
| d | deflection of particle | [m] |
| $d_p$ | diameter of particle | [m] |
| $d_{co}$ | diameter of cone | [m] |
| $d_w$ | wire diameter | [m] |
| D | diffusion coefficient | [$m_2$/s] |
| e | unit charge | [C] |
| E | kinetic energy of particle | [J] |
| $E_1$ | electric field at electrode | [V/m] |
| h | heat transfer coefficient | [W/$m_2$·K] |
| HW | halfwidth of the spectrum | [Hz] |
| $I_\lambda$ | emitted flame intensity | [W/$m^2$] |
| $I_{b\lambda}$ | black-body intensity | [W/$m^2$] |
| $J_w''$ | particle flux | [#/$m^2$·s] |
| k | Boltzman constant | [J/K] |
| K | mobility parameter | [-] |
| $l_c$ | length of capacitor | [m] |
| $l_f$ | distance capacitor- blend | [m] |
| $l_g$ | distance between grids | [m] |
| L | length of tube | [m] |
| m | complex refractive index of the particle | [-] |
| $m_p$ | mass of particle | [kg] |
| N | number of particles per unit volume | [-/$m^3$] |
| $n_e$ | number of unit charges | [-] |
| P | penetration | [-] |
| $Q_{vv}$ | scattered cross-section | [$m^{-1}$·$str^{-1}$] |
| $Q_{ext}$ | extinction efficiency factor | [-] |
| r | radius of disk-sink/probe | [m] |
| $r_p$ | particle radius | [m] |
| $r_1$ | radius of collection rod | [m] |
| T | absolute temperature | [K] |
| $t_f$ | residence time | [s] |
| U | accelerating voltage | [V] |
| $v_p$ | velocity of particle | [m/s] |
| $v_\infty$ | unperturbed velocity | [m/s] |
| $v_y$ | velocity in y-ditection | [m/s] |
| W | width of slab (in double extinction technique) | [m] |
| $Z_p$ | mobility of particle | [$m^2$/V·s] |

**Greek**

| | | |
|---|---|---|
| $\alpha$ | sampling ratio | [-] |
| $\beta$ | pre-exponential factor | [V] |
| $\beta_\lambda^p$ | particle extinction coefficient | [$m^{-1}$] |
| $\beta_\lambda^g$ | gas extinction coefficient | [$m^{-1}$] |
| $\delta_t$ | thickness of thermal boundary layer | [m] |
| $\delta$ | shift of velocity profile | [m] |
| 1-$\epsilon$ | porosity of screen | [-] |
| $\eta$ | viscosity | [Pa·s] |
| $\theta$ | scattering angle | [-] |
| $\kappa$ | d ln($\lambda$)/d ln T | [-] |
| $\kappa_\kappa^p$ | particle absorption coefficient | [$m_{-1}$] |
| $\kappa_\kappa^g$ | gas absorption coefficient | [$m_{-1}$] |
| $\lambda_0$ | wavelength of the incident beam | [m] |
| $\lambda$ | heat conductivity | [W/m·K] |

| | | |
|---|---|---|
| $\mu$ | deposition parameter | [-] |
| $\nu_g$ | kinematic viscosity of the gas | [m/s] |
| $\rho$ | density | [kg/m$^3$] |
| $\tau$ | decay time | [s] |
| $\tau_e$ | exposure time | [s] |
| $\tau_r$ | characteristic reaction time | [s] |
| $\tau_q$ | quench time | [s] |
| $\tau_{cc}$ | transmittance | [-] |
| $\Phi$ | volumetric flow rate | [m$^3$/s] |
| $\Phi_w^{"}$ | heat flux | [W/m$_2$] |
| $\Omega$ | instrument transfer function | [-] |

**Dimensionless numbers**

$$Re \quad \frac{\rho \cdot v \cdot d}{\eta}$$

$$Sc \quad \frac{\eta}{\rho \cdot D}$$

$$\Pi_1 \quad \frac{d_{co}}{v_0 \cdot \tau_r}$$

$$\mu \quad \frac{D \cdot L}{\Phi_v}$$